Fractal Aggregates in Protein Crystal Nucleation

Bin Chen,* Ricky B. Nellas, and Samuel J. Keasler

Department of Chemistry, Louisiana State University, Baton Rouge, Louisiana 70803-1804

Received: December 6, 2007

Monte Carlo simulations of homogeneous nucleation for a protein model with an exceedingly short-ranged attractive potential yielded a nonconventional crystal nucleation mechanism, which proceeds by the formation of fractal, low-dimensional aggregates followed by a concurrent collapse and increase of the crystallinity of these aggregates to become compact ordered nuclei. This result corroborates a recently proposed two-step mechanism for protein crystal nucleation from solution.

1. Introduction

Understanding the nucleation phenomenon, in which a new phase is born out of a metastable supersaturated phase, has important implications in many scientific and technological areas. As applied to proteins, the importance of this problem has been recently re-emphasized by the rapid growth of structural proteomics.[1] In particular, the preparation of high-quality crystals from protein solutions has become a bottleneck for the structural determination of new classes of biomolecules.[2] Therefore, over the past decade, finding the optimal conditions and/or physical mechanisms for enhanced protein crystal nucleation has been the major theme for a great deal of protein crystallization research, which, in turn, has illustrated a rather intriguing side of this phenomenon.

A decade ago, George and Wilson[3] demonstrated that the second osmotic virial coefficient could be used as an effective predictor for achieving successful crystallization of proteins. For a variety of proteins, the solvent conditions that favor crystallization confine B_2 to a narrow range of small negative values. While large negative values of B_2 lead to protein aggregation instead of crystallization, large positive values of B_2 disable the crystallization completely. This interesting correlation immediately inspired some theoretical work. Rosenbaum, Zamora, and Zukoski[4,5] showed that this surprising result arises partly from the unusual phase behavior of protein solutions, i.e., the existence of a metastable fluid−fluid coexistence curve below the fluid−solid coexistence curve, due to the short-range attractive interactions between proteins (see Figure 1).[6−8] In addition, they mapped the solvent conditions onto the phase diagram of protein solutions and observed that proteins crystallize in a narrow temperature range, equivalent to the narrow range of small negative B_2.[8,9]

To gain microscopic insight into the physical mechanism of this process, ten Wolde and Frenkel[8] performed the first protein crystal nucleation simulation. They found that the free energy barrier for crystal nucleation is strongly reduced at the metastable fluid−fluid critical point (CP). The underlying physical mechanism was attributed to the large density fluctuations around the CP, which lead to the initial formation of liquid-like droplets (density fluctuation) followed by crystal nucleation (structure fluctuation) inside these high-density droplets. A similar conclusion was also drawn by Talanquer and Oxtoby with density functional theory.[10] However, the prediction of nucleation enhancement at the CP was soon questioned by other theoretical and experimental work.[11−13] The main problem is that protein solutions gel at the CP as a result of the high concentration and the associated high viscosity. In addition, experiments using lower concentrations of lysozyme also observed crystal nucleation enhancement, but at temperatures close to the fluid−fluid coexistence temperatures.[2] The fact that this enhancement follows along the fluid−fluid coexistence curve at different concentrations led Vekilov[14] to suggest that density fluctuations (i.e., the formation of liquid-like droplets) are not just a part of the crystal nucleation mechanism around the CP. Therefore, a general two-step mechanism was proposed in which density fluctuations occur first, followed by the structural fluctuations, over a much broader range of phase space than previously thought. Although this mechanistic proposal provides an explanation of the protein crystal nucleation enhancement observed there under different temperature conditions, it requires further theoretical support, as, until now, the superposition of these two fluctuations was only revealed at the CP.[8] More importantly, many of the microscopic details regarding how these two fluctuations are superimposed onto each other remain unclear. Even simpler questions about the nature of these liquid-like intermediates have barely been addressed. For example, what do the quasi-droplets look like? Could they be doubly metastable, i.e., metastable with respect to both the solution and the crystals as Vekilov and coworkers suggested?[14,15] Also, what are the relative barriers that the two fluctuations have to overcome in the crystal nucleation landscape?

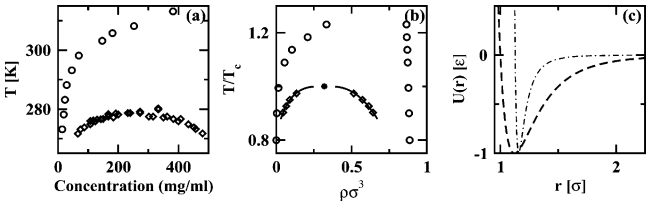

Figure 1. (a) A typical protein phase diagram showing a metastable fluid−fluid coexistence region (diamonds) below the solubility line (circles).[6,7] (b) A model potential with short-range attractive interactions reproducing this behavior.[8] (c) Comparison of this potential (dashed−dotted line) to the common LJ potential (dashed line).

To address these questions, we extended the aggregation-volume-bias Monte Carlo approach, which has led to our recent

* Corresponding author. E-mail: binchen@lsu.edu.

10.1021/jp8002728 CCC: $40.75
Published on Web 03/22/2008

success in vapor−liquid nucleation (e.g., see refs 16 and 17), to the computation of the free energy landscape involved in protein crystal nucleation. Presented in the next section are the technical details of this extension followed by a brief description of the simulations carried out in this study. The simulation results are presented and discussed in section 3, and section 4 provides concluding remarks.

2. Simulation Methods and Details

The simulation method used here is built upon the AVUS-HR technique[18,19] that was recently pioneered by combining aggregation-volume-bias Monte Carlo (AVBMC),[20,21] configurational-bias Monte Carlo (CBMC),[22−24] umbrella sampling (US),[25] and histogram reweighting (HR).[26,27] The advantage of this method in studying rare nucleation events lies in its ability to overcome the large free energy barriers (or low probabilities for the occurrence of nuclei near the critical size) via the use of US, and the inherent micro-heterogeneity of the phase space (i.e., coexistence of clusters and monomers) with AVBMC.[28] In particular, through direct particle swaps between the cluster and the mother phase, AVBMC greatly expedites both cluster growth and destruction by (i) circumventing the long time-scale diffusion process required for cluster growth in the conventional Metropolis[29] Monte Carlo scheme and molecular dynamics; and (ii) enhancing the acceptance rate for the reverse move to satisfy the detailed balance condition (i.e., the bias introduced in the cluster growth enters the acceptance rule, which compensates for the energetic penalty from cluster destruction). Once frequent cluster growth and destruction are achieved, it is desirable to single out one cluster from the whole system and turn a global problem into a local one.[28,30] This allows us to greatly reduce the size of the system required for the simulation, and the distribution information obtained from this single cluster can be used to derive the cluster probability distribution for the whole system. The incorporation of CBMC further enhances its efficiency and enables the extension of this method to molecules with articulated structures. HR is exploited to make predictions for a range of temperatures and partial pressures.

While the cluster size serves as the major order parameter in our previous vapor−liquid nucleation studies, the reaction coordinates for the crystal nucleation described here also consist of the compactness of the cluster (described by its radius of gyration, r_g) and its crystallinity (described by the orientationally independent Steinhardt order parameter Q_6).[30−33] The size of the cluster is determined through the Stillinger cluster criteria with a distance cutoff of 1.23σ.[15,28,34] This set of order parameters were also inspired by the schematic illustration of the previously proposed two-step mechanism (see Figure 6 in ref 14), where the density, size, and structure of the cluster were considered as reaction coordinates in the nucleation of protein crystals. It should be noted that, in ref 8, the order parameters were confined to the size of some *high-density* cluster, either liquid-like or crystalline, which precludes the possibility of observing *low-density* structures on the nucleation path. Compared to theirs, our nucleation free energy (NFE) landscape also expands along the density coordinate, i.e., r_g, since the crystalline order parameter Q_6, computed for only the cluster and not the entire system, was found to correlate with the size of the largest crystallite. The same protein model used in their work was investigated here to examine the relevance of the density coordinate in the crystal nucleation process. It is a simplified, effective pair potential that includes both direct and solvent-induced interactions between the globular proteins.[8] The most important feature of this model is its exceedingly short-ranged attractive interactions (see Figure 1c) that are essential to capture the general phase behavior of protein solutions (i.e., the presence of a metastable fluid−fluid coexistence region beneath the solubility line, see Figure 1b). In particular, the attractive well is much narrower compared to the typical Lennard-Jones (LJ) type of potential expected for small molecular systems (such as argon and methane), which are known to have a stable fluid−fluid coexistence region. As shown previously,[35−37] the relative narrowness of the interaction potential controls whether a stable, dense fluid phase is present. This short-ranged attractive interaction is expected to be general for many nanometer-sized particles (e.g., fullerenes, colloids, proteins, etc.) and arises naturally from the fact that the ranges of the various interactions between the particles are on similar atomic length scales (i.e., a few angstroms), irrespective of the overall size of the molecule, but become shorter compared to the size of the molecule for larger particles.[14,38−41]

All simulations were carried out using the isobaric−isothermal version of the nucleation algorithm[28] unless explicitly noted. Three temperatures were selected near the critical temperature (T_c) of 0.421, which was determined from Gibbs ensemble Monte Carlo simulations.[42−44] They were referred to as 0.90, 0.95, and 1.0 T_c, corresponding to the actual temperatures of 0.38, 0.40, and 0.42, respectively (in reduced units). For each temperature, the pressure was chosen such that the density of the fluid phase (or, equivalently, the volume fraction of the molecules) was around the coexistence density of the dilute fluid phase at $T = 0.90\ T_c$, which is 0.046 in reduced units. At $T = 1.0\ T_c$, an additional simulation was also carried out at a higher pressure, which yields a reduced density of 0.138, which is still lower than the critical density but is already near the boundary where gelation can occur (see the experimental protein phase diagram shown in ref 14). The pair potential was truncated at 4.75σ where the interaction energy is $\mathcal{O}(10^{-6}\epsilon)$. The upper-bound of the radius of gyration and cluster size were chosen carefully to ensure that the most important part of the free energy landscape is fully sampled (including the stable regions and the saddle point connecting these regions). While 864 particles were used for the simulation at $T = 0.90\ T_c$, 3000 particles were used for the simulations at higher temperatures since larger and more extended clusters were investigated there. These system sizes were found to be large enough to avoid percolation of the clusters through the periodically replicated system. Since both Q_6 and r_g are continuous variables, in collecting the cluster distribution information, bin widths of 0.01 and 0.1σ were used for constructing the histograms along these two coordinates. Each cluster of a specific size (and structure) was visited at least 10^4 times.

Although one simulation box was used, the system could be viewed as being composed of two parts: a cluster (which is our central focus) surrounded by a mother phase. Three different kinds of Monte Carlo moves were used to sample the phase space: particle exchanges between these two parts of the system via AVBMC swaps, translations, and volume moves. The frequency of the volume moves was fixed at one per Monte Carlo cycle (one Monte Carlo cycle consists of N moves where N is the system size), and its maximum displacement was adjusted to yield acceptance rates of 50%. During the volume move, the central cluster is allowed to change and may even gain or lose molecules, but the first molecule in the old cluster maintains its position in the new cluster to ensure microscopic reversibility.[45] The rest of the moves were roughly equally divided between translations and AVBMC swaps. The maximum displacement of the translations was fixed at 0.2σ for the

cluster or 5σ for the mother phase (larger values were used for the latter part of the system as it is relatively more dilute). If a translational move resulted in a change of the cluster size, it was rejected. There are two types of AVBMC swaps: particle insertion and deletion from the cluster. A typical AVBMC swap proceeds as follows: (i) randomly select the move type as an insertion or a deletion with equal probabilities; (ii) randomly select a particle j from the n particles contained by the cluster to act as a target for the swap move; (iii) if an insertion is selected, one particle is randomly selected from the mother phase and transferred into the bonded region of particle j, or, if it is a deletion, then one particle is randomly selected from the N_{in} particles within the bonded region of particle j and transferred into the mother phase; (iv) calculate the potential energy difference between the initial state $\mathcal{A}$ and the trial state $\mathcal{B}$, $\Delta E = E_{\mathcal{B}} - E_{\mathcal{A}}$; and (v) accept this move with the following set of acceptance probabilities:

(a) if it is an insertion,

$$\mathrm{acc}(\mathcal{A} \rightarrow \mathcal{B}) = \min\left[1, \frac{V_{in} \times n \times (N-n) \times \exp(-\Delta E/k_B T)}{(N_{in}+1) \times (n+1) \times V}\right] \quad (1)$$

(b) if it is a deletion,

$$\mathrm{acc}(\mathcal{A} \rightarrow \mathcal{B}) = \min\left[1, \frac{N_{in} \times n \times V \times \exp(-\Delta E/k_B T)}{V_{in} \times (n-1) \times (N-n+1)}\right] \quad (2)$$

where V_{in} is the volume of the bonded region (in this case, a spherical volume centered on particle j with a radius of 1.23σ, the same distance used for the Stillinger cluster criterion), and V is the volume of the entire system. The use of V rather than $V - V_{cluster}$ (with $V_{cluster}$ denoting the volume of the cluster) in eq 1 leads to a reduction of the acceptance probabilities for the insertion move by a factor of $V_{cluster}/V$, which is small considering that the cluster only occupies a very small fraction of the total volume. Also, this reduction is compensated exactly by a decrease of the acceptance probabilities for the deletion move (i.e., for simplicity in the "deletion" move, the new position of this molecule is allowed to be anywhere in the simulation box, but those deletions that happen to be placed back in the cluster volume are rejected).[45]

3. Simulation Results and Discussions

All simulations were started by iterating the NFEs of the clusters along the cluster size coordinate first and were later expanded along the other two coordinates (r_g and Q_6). The sole use of the Stillinger cluster size as the order parameter yielded only disordered aggregates for the simulation conditions considered here, as mostly low Q_6 values were found for these clusters. Further analysis of r_g revealed that these clusters are fractal, low-dimensional aggregates. The evidence came from the log−log plot of the aggregation number versus the r_g parameter (see Figure 2). For compact, three-dimensional objects, a slope of 3 would be expected from this plot. But for the model protein, a value of close to 2 was found over almost the entire range of cluster sizes sampled. Only at the lowest temperature did the fractal aggregates show a tendency to collapse into more compact objects (see the dotted line in Figure 2). The radius of gyration curves obtained at 1.0 T_c for both low and high concentration cases show similar tilts toward larger clusters, which were due to the limited range of r_g ($<8\sigma$) sampled here. More importantly, the fractal nature of these aggregates is fairly insensitive to the protein concentration (with the two curves nearly coincident with each other).

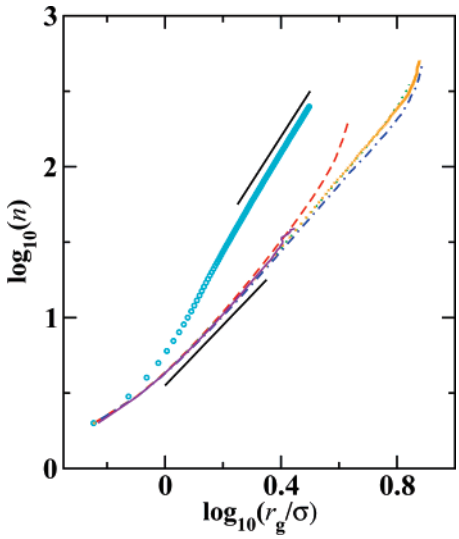

Figure 2. Log−log plot of cluster size versus radius of gyration where the data show a slope of close to 2 (more precisely, <2 for small aggregates and >2 for large aggregates) for this model protein at $T =$ 0.90 (red dashed), 0.95 (green dotted), and 1.0 T_c (blue dashed-dotted line and orange crosses for the low and high concentration cases, respectively) versus 3 for LJ (cyan circles). Results obtained from the additional simulations using the more conventional approach (see text) at $T = 0.95\ T_c$ are shown as the purple solid line. The two black solid lines with slopes of 2 (lower) and 3 (upper) are drawn as a guide.

Additional simulations were carried out using the more conventional approach where the statistical average of the r_g value was interpreted from all clusters formed in the system (and for all configurations). Since our focus is no longer restricted to a single cluster, we used AVBMC2 described in ref 21 to allow for an efficient sampling of the growth and destruction for all clusters present in the system and no US (as the implementation of US would be more troublesome for this multicluster approach).[28] As shown in Figure 2 for the $T = 0.95$ T_c case, good agreement was found between the data obtained from these new simulations and those using the single-cluster approach. However, without the use of US biasing potentials, only small clusters of a limited size-range can be sampled (which is the reason why the data are only available for clusters up to a size of about 50).[28]

While for proteins, fractal, low-dimensional aggregates exist for a very wide cluster-size range, for normal molecular systems that interact with an LJ potential, the transition into compact structures happens immediately at clusters consisting of only a few molecules. From this comparison, it is clear that the short-range nature of the attractive interactions (see Figure 1c) is responsible for the formation of the fractal, low-dimensional aggregates observed for proteins. In particular, the energetic gain in the transition from fractal to compact aggregates is greatly reduced as compared to particles interacting with a much longer range (such as LJ), and cannot compensate for the entropic loss during the collapse unless the cluster size is large enough. As the fractal aggregates are favored entropically, increasing the temperature would make them even more stable than the compact ones. This would not only lead to higher r_g values for a given cluster size but also shift the collapse transition to even larger clusters, which is consistent with the data shown in Figure 2. On the other hand, since the disordered aggregates are predominantly fractal and loosely packed while the fully ordered crystals are highly compact, the disorder-to-order transition

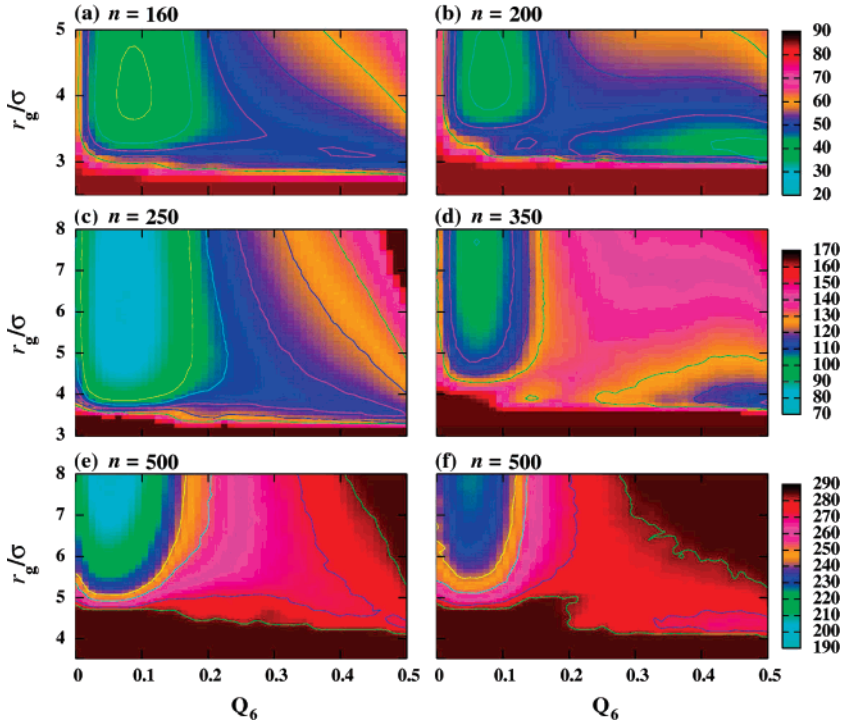

Figure 3. Contours of the two-dimensional NFEs (in units of k_BT) as a function of the Steinhardt order parameter Q_6 and radius of gyration r_g for clusters at a constant size n as specified. The top, middle, and bottom two panels are for $T = 0.90$, 0.95, and 1.0 T_c, respectively. The three panels on the left are drawn at a cluster size when the crystalline phase is about to develop into a stable region, termed as n_t (see text). The data in panel f are shifted by 210 k_BT and represent the high concentration case. The contour levels with constant NFE values are depicted as lines for a clear view of the NFE profiles near the saddle point, starting from 36, 100, or 243 k_BT (shown as orange lines) with an interval of 6, 8, or 10 k_BT for the top, middle, and bottom two panels, respectively.

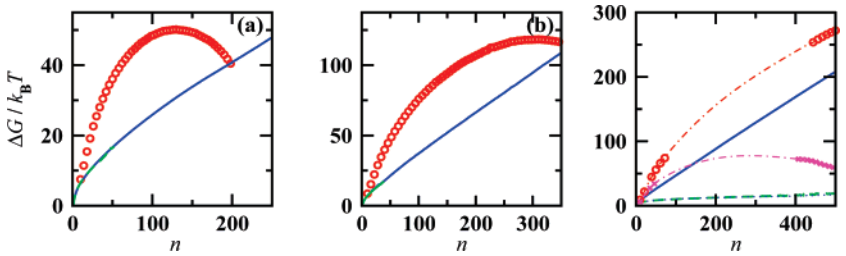

Figure 4. NFEs as a function of the cluster size for disordered (blue solid lines) or ordered (red circles; with Q_6 above 0.45) aggregates obtained from the simulations at (a) $T = 0.90$ T_c, (b) $T = 0.95$ T_c, and (c) $T = 1.0$ T_c. Magenta crosses and a blue dotted line represent the results obtained for the high-concentration case at $T = 1.0$ T_c. The dashed-dotted lines in panel c represent the interpolated results based on the converged NFEs at low and high cluster-sizes. Results obtained from the additional simulations using the more conventional approach without the use of umbrella biasing potentials are shown as green dashed lines.

would have to incur a change along the density coordinate (r_g) under the simulation conditions considered here.

The addition of the r_g and Q_6 coordinates to the construction of the NFE landscape reveals a stable crystalline region toward larger clusters, which can be visualized by plotting the NFE data as a function of these two coordinates for a specific cluster size (see Figure 3). From these contour plots it is evident that, at each temperature, there is a size threshold (n_t) beyond which the crystalline-like clusters start to evolve steadily into a stable phase. Below n_t, only one stable region with low Q_6 values and high r_g values (which corresponds to the disordered fractal state) can be found on the NFE maps. Therefore, n_t can serve as an initial guide to where the disordered-to-ordered transition would take place on the NFE landscape. This threshold size is not necessarily the critical size of the ordered nucleus (n_c) since the NFE values may go either up or down along the cluster-size coordinate for these ordered structures. The value of n_c can be estimated by plotting the NFE data as a function of the cluster size for clusters with a relatively high degree of crystallinity (see Figure 4). Also included in Figure 4 are the NFE data interpreted from the cluster-size distribution of the entire system, obtained from those additional simulations described above (i.e., without the use of US but with AVBMC2). As shown in Figure 4, these NFE data were again found to be consistent with those interpreted from the simulations using the single-cluster approach. However, in the absence of the US biasing potential, reliable data can be only obtained for a limited NFE range, as clusters with NFE above 20 k_BT can barely be sampled.[28]

It is evident from Figure 4 that, at a given protein concentration, an increase in temperature would shift both n_c and n_t to higher values but by a larger magnitude for n_c compared to n_t. For example, at $T = 0.90$ T_c, n_c was found to be lower than n_t, with a value of 130 for n_c versus 160 for n_t. In contrast, at $T = 0.95$ T_c, n_c (310) was already higher than n_t (250). On the other hand, increasing the concentration would reduce n_c but barely affect n_t (see Figure 3e,f). Thus, the relative values of these two numbers can be changed by the tuning of either temperature or concentration. Most importantly, this switch from n_t being larger to n_c being larger implies a subtle mechanistic change in

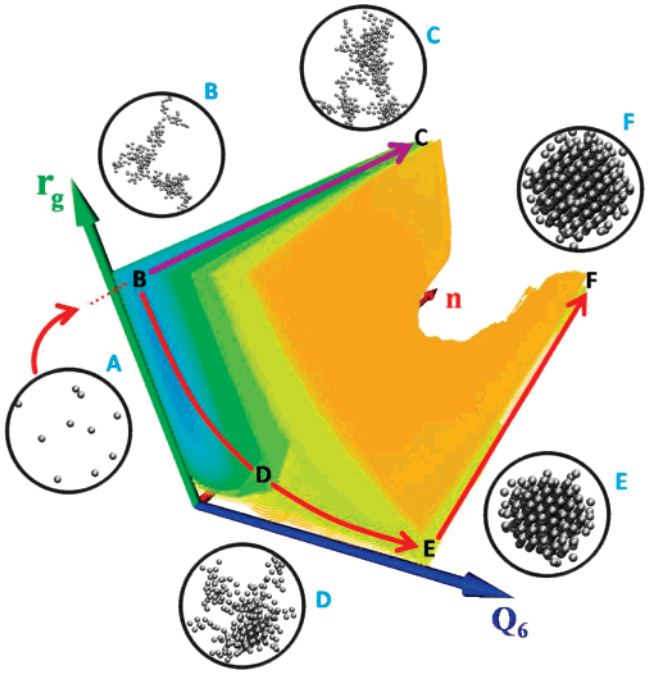

Figure 5. Illustration of a crystal nucleation path consisting of steps AB, BDE, and EF on the NFE landscape obtained at $T = 0.95\ T_c$. For clarity, only the part of landscape for clusters larger than n_t (= 250) and with NFE values below 100 k_BT or at discretized NFE values of 108 (yellow−green layer), 116 (yellow layer), 124 k_BT (orange layer) is displayed. Amorphous aggregation proceeds further after point B on path BC. Representative snapshots are shown for each point marked on this landscape.

the crystal nucleation process. As shown in Figure 5, when n_c is larger than n_t, crystal nucleation will mostly proceed via three steps: (i) a fluctuation along the cluster size coordinate (for disordered structures), (ii) a disorder-to-order transition (fluctuation along both r_g and Q_6 coordinates), and (iii) another fluctuation along the cluster size coordinate (for ordered structures this time) until it reaches the critical crystal nucleus size. On the contrary, for cases when n_c is smaller than n_t, the last step is no longer critical for the crystal nucleation process, as it occurs in the crystal growth stage, leading to a simplified two-step mechanism. The latter scenario to some extent resembles the crystal nucleation mechanism proposed by Vekilov[14] (with nucleation initiated by the growth of disordered aggregates, followed by the formation of ordered structures inside these aggregates after they reach a certain size). However, in this mechanistic proposal, the second step was depicted along the crystalline structure coordinate only. In our simulation, the disorder-to-order transition is also accompanied by a collapse of these fractal objects into denser aggregates. As the disordered protein aggregates are more fractal at higher temperatures, this coupling becomes even more obvious (see Figure 3).

Visual inspection of the cluster configurations further confirms the fractal nature of the disordered aggregates (see snapshots included in Figure 5). Some of the low-density structural motifs are reminiscent of the low-dimensional, chain-like species formed by molecules interacting through anisotropic interactions such as dipolar hard-spheres. The structural resemblance between these two cases is remarkable considering that no directional forces are present in the protein model employed here, and can be only explained by their exceedingly narrow-ranged attractions (either restricted by the radial separation or by the orientational arrangement). While for dipolar hard-sphere systems it has been speculated that the chain-like association may preclude the presence of a stable fluid−fluid coexistence curve,[46] for this model protein, the disappearance of a stable fluid−fluid coexistence curve does happen concurrently with the preferred formation of fractal, low-dimensional species in the aggregation. Direct evidence of the formation of low-dimensional protein aggregates has been recently provided by both atomic force microscopy[47] and multi-angle light scattering experiments.[48,49] In particular, in the latter work, the fractal dimensionality was evaluated, which was found to be consistently low for the initial aggregates formed, irrespective of the protein concentration, and slowly increases to 3 only when the aggregates are sufficiently large. In contrast, most nucleation theories to date rely on an assumption of a spherical nucleus structure. As the shape of the nucleus could affect its energy and thus the rate of formation, the finding of non-spherical loosely packed species poses a grand challenge to the validity of applying those theories to derive the size and free energy of the critical nuclei.[50]

Finally, these simulations are able to explain the decrease of the nucleation rate as the temperature is increased away from the coexistence temperature, with the lowest barrier obtained at $T = 0.90\ T_c$, which is closest to the coexistence temperature for the specified concentration. Additional simulations at a lower temperature of 15% below T_c indicate spontaneous aggregation, even without the use of biasing potentials. The formed aggregates are compact and liquid-like. Under such conditions, the almost barrierless aggregation would lead to a rapid formation of large disordered structures, while the crystal nucleation inside these aggregates would be slowed down or arrested by the highly concentrated local environment, which makes it difficult to obtain high-quality protein crystals,[49] and sometimes also causes the gelation problem observed for protein solutions.[14] On this basis, it is tempting to suggest that the conditions that favor crystal nucleation would be those that greatly lower the NFE values for the protein clusters (by either decreasing the temperature or increasing the concentration) but not to the level when large compact liquid-like aggregates start to form. The loosely packed, low-dimensional aggregates appear to be the important intermediates. Therefore, favorable formation and stabilization of these species (specifically, by preventing them from growing into larger and denser liquid-like clusters) may be the key for protein crystal nucleation enhancement. However, it should be realized that the model employed here is very simplified and does not allow a realistic consideration of such kinetic factors as diffusion and gyration. Also, these factors could only be fully taken into account via dynamical simulations, but the presence of the aggregation process is a challenge for even the most sophisticated techniques available, e.g., transition path sampling.[51] For concentrated solutions, additional issues arise from the low-barrier aggregation (see Figure 4c), which may lead to the formation of multiple clusters and a quick exhaustion of monomers. When these rapidly formed clusters are still not large enough to crystallize (i.e., the cluster size is below n_t, which is more likely to happen at intermediate concentrations), the development of the crystalline structure would require further cluster growth, which can only proceed via the much slower cluster−cluster aggregation or transfer of protein molecules between clusters, making the whole process diffusion-limited.[49] On the other hand, a full description of such cluster−cluster aggregations/interactions can only be provided by simulations employing much larger systems than presented here. Given these considerations, further development of more realistic models and/or advanced methods are needed for an ultimate probing of protein crystal nucleation in solution.

4. Conclusions

In conclusion, we extended the recently developed AVUS-HR technique to the study of the crystal nucleation process encountered by a model protein that interacts with an exceedingly short-ranged isotropic attractive potential. The most important finding of this study is the formation of fractal, low-dimensional aggregates that exist for a much wider cluster-size range than normal molecular systems (that interact via an LJ type of potential).

Acknowledgment. We thank Prof. Ilja Siepmann for many stimulating discussions. Financial support from the LSU start-up fund, the National Science Foundation (CHE/MCB-0448918), the Louisiana Board of Regents Support Fund (LEQSF(2005-08)-RD-A-02), the Petroleum Research Fund administered by the American Chemical Society (Grant No. 41933-G9), and a Council on Research Summer Stipend Award from the LSU Office of Research and Graduate Studies is gratefully acknowledged. Part of the computer resources were provided by the Center for Computation and Technology, the Office of Computing Services at LSU, and the Louisiana Optical Network Initiative.

References and Notes

(1) McPherson, A. *Crystallization of Biological Macromolecules*; Cold Spring Harbor: New York, 2002.
(2) Galkin, O.; Vekilov, P. G. *J. Am. Chem. Soc*. **2000**, *122*, 156.
(3) George, A.; Wilson, W. W. *Acta Crystallogr., Sect. D* **1994**, *50*, 361.
(4) Rosenbaum, D. F.; Zamora, P. C.; Zukoski, C. F. *Phys. Rev. Lett.* **1996**, *76*, 150.
(5) Rosenbaum, D. F.; Zukoski, C. F. *J. Cryst. Growth* **1996**, *169*, 752.
(6) Berland, C. R.; Thurston, G. M.; Kondo, M.; Broide, M. L.; Pande, J.; Ogun, O. O.; Benedek, G. B. *Proc. Natl. Acad. Sci. U.S.A.* **1992**, *89*, 1214.
(7) Broide, M. L.; Berland, C. R.; Pande, J.; Ogun, O. O.; Benedek, G. B. *Proc. Natl. Acad. Sci. U.S.A.* **1991**, *88*, 5660.
(8) ten Wolde, P. R.; Frenkel, D. *Science* **1997**, *277*, 1975.
(9) Hagen, M. H. J.; Frenkel, D. *J. Chem. Phys*. **1994**, *101*, 4093.
(10) Talanquer, V.; Oxtoby, D. W. *J. Chem. Phys*. **1998**, *109*, 223.
(11) Evans, R. M. L.; Poon, W. C. K.; Cates, M. E. *Europhys. Lett*. **1997**, *38*, 595.
(12) Soga, K. G.; Melrose, J. R.; Ball, R. C. *J. Chem. Phys*. **1999**, *110*, 2280.
(13) Galkin, O.; Vekilov, P. G. *Proc. Natl. Acad. Sci. U.S.A.* **2000**, *97*, 6277.
(14) Vekilov, P. G. *J. Cryst. Growth* **2005**, *275*, 65.
(15) Gliko, O.; Pan, W.; Katsonis, P.; Neumaier, N.; Galkin, O.; Weinkauf, S.; Vekilov, P. G. *J. Phys. Chem. B* **2007**, *111*, 3106.
(16) Nellas, R. B.; Chen, B.; Siepmann, J. I. *Phys. Chem. Chem. Phys.* **2007**, *9*, 2779.
(17) Nellas, R. B.; Chen B. *Phys. Chem. Chem. Phys*. **2007**, *10*, 506.
(18) Chen, B.; Siepmann, J. I.; Klein, M. L. *J. Phys. Chem. A* **2005**, *109*, 1137.
(19) Nellas, R. B.; McKenzie, M. E.; Chen, B. *J. Phys. Chem. B* **2006**, *110*, 18619.
(20) Chen, B.; Siepmann, J. I. *J. Phys. Chem. B* **2000**, *104*, 8725.
(21) Chen, B.; Siepmann, J. I. *J. Phys. Chem. B* **2001**, *105*, 11275.
(22) Siepmann, J. I.; Frenkel, D. *Mol. Phys*. **1992**, *75*, 59.
(23) Frenkel, D.; Mooij, G. C. A. M.; Smit, B. *J. Phys.: Condens. Matter* **1992**, *4*, 3053.
(24) Martin, M. G.; Siepmann, J. I. *J. Phys. Chem. B* **1999**, *103*, 4508.
(25) Torrie, G. M.; Valleau, J. P. *Chem. Phys. Lett*. **1974**, *28*, 578.
(26) Wilding, N. B. *Phys. Rev. E* **1995**, *52*, 602.
(27) Potoff, J. J.; Panagiotopoulos, A. Z. *J. Chem. Phys*. **1998**, *109*, 10914.
(28) Chen, B.; Siepmann, J. I.; Oh, K. J.; Klein, M. L. *J. Chem. Phys*. **2001**, *115*, 10903.
(29) Metropolis, N.; Rosenbluth, A. W.; Rosenbluth, M. N.; Teller, A. H.; Teller, E. *J. Chem. Phys*. **1953**, *21*, 1087.
(30) ten Wolde, P. R.; Ruiz-Montero, M. J.; Frenkel, D. *Faraday Discuss.* **1996**, *104*, 93.
(31) Steinhardt, P. J.; Nelson, D. R.; Ronchetti, M. *Phys. Rev. B* **1983**, *28*, 784.
(32) Moroni, D.; ten Wolde, P. R.; Bolhuis, P. G. *Phys. Rev. Lett*. **2005**, *94*, 235703.
(33) Trudu, F.; Donadio, D.; Parrinello, M. *Phys. Rev. Lett.* **2006**, *97*, 105701.
(34) Stillinger, F. H. *J. Chem. Phys*. **1963**, *38*, 1486.
(35) Chen, B.; Siepmann, J. I.; Karaborni, S.; Klein, M. L. *J. Phys. Chem. B* **2003**, *107*, 12320.
(36) Noro, M. G.; Frenkel, D. *J. Chem. Phys*. **2000**, *113*, 2941.
(37) Vliegenthart, G. A.; Lekkerkerker, H. N. W. *J. Chem. Phys*. **2000**, *112*, 5364.
(38) Asherie, N.; Lomakin, A.; Benedek, G. B. *Phys. Rev. Lett.* **1996**, *77*, 4832.
(39) Casselyn, M.; Perez, J.; Tardieu, A.; Vachette, P.; Witz, J.; Delacroix, H. *Acta Crystallogr., Sect. D: Biol. Crystallogr*. **2001**, *57*, 1799.
(40) Tardieu, A.; Verge, A. L.; Malfois, M.; Bonnette, F.; Finet, S.; Ries-Kaut, M.; Belloni, L. *J. Cryst. Growth* **1999**, *196*, 193.
(41) Muschol, M.; Rosenberger, F. *J. Chem. Phys*. **1995**, *103*, 10424.
(42) Panagiotopoulos, A. Z.; Quirke, N.; Stapleton, M.; Tildesley, D. J. *Mol. Phys*. **1988**, *63*, 527.
(43) Smit, B.; de Smedt, P.; Frenkel, D. *Mol. Phys*. **1989**, *68*, 931.
(44) Chen, B.; Siepmann, J. I.; Klein, M. L. J. *Phys. Chem. B* **2001**, *105*, 9840.
(45) Chen, B.; Siepmann, J. I.; Oh, K. J.; Klein, M. L. *J. Chem. Phys*. **2002**, *116*, 4317.
(46) Ganzenmüller, G.; Camp, P. J. *J. Chem. Phys.* **2007**, *126*, 191104.
(47) Yau, S.-T.; Vekilov, P. G. *Nature* **2000**, *406*, 494.
(48) Onuma, K.; Watanabe, A.; Kanzaki, N.; Kubota, T. *J. Phys. Chem. B* **2006**, *110*, 24876.
(49) Onuma, K.; Kanzaki, N. *J. Cryst. Growth* **2007**, *304*, 452.
(50) Oxtoby, D. W. *Nature* **2000**, *406*, 464.
(51) Zahn, D. *J. Phys. Chem. B* **2006**, *110*, 19601.